ISSN 0884-5913, Kinematics and Physics of Celestial Bodies, 2018, Vol. 34, No. 2, pp. 68–81. © Allerton Press, Inc., 2018.
Original Russian Text © M.N. Pasechnik, 2018, published in Kinematika i Fizika Nebesnykh Tel, 2018, Vol. 34, No. 2, pp. 25–45.

SOLAR PHYSICS

Spectral Study of Ellerman Bombs. Photosphere

M. N. Pasechnik

Main Astronomical Observatory, National Academy of Sciences of Ukraine, Kyiv, 03143 Ukraine

e-mail: rita@mao.kiev.ua

Received October 5, 2017

Abstract—The results of analysis of spectral observations of two Ellerman bombs (EB-1 and EB-2), which were formed and have evolved in the area of emerging magnetic flux in active region (AR) NOAA 11024, are presented. Spectral data with high spatial and temporal (approximately 3 s) resolution were obtained using the THEMIS French–Italian solar telescope on July 4, 2009. The observation duration was 20 min. The spectral region of $\lambda \approx 630$ nm with photospheric lines forming in a wide altitude range (neutral iron lines Fe I λ 630.15, 630.25, and 630.35 nm and titanium line Ti I λ 630.38 nm) was examined. The brightness of EB-1 decreased in the process of observations, while the brightness of EB-2 increased. The profiles of metal lines determined at different stages of EBs evolution were asymmetric. This asymmetry was more pronounced in lines that had formed in the lower photospheric layers and often had profiles with several components. The half-width of profiles increased with a reduction in their central depth. The variation of central intensities of Fraunhofer lines in the spectra of EBs and their vicinity at different stages of EB evolution was analyzed. The EBs formed in intergranular lanes. An increase in the core intensity of all the studied photospheric lines was correlated spatially with an increase in the wings intensity of the H_α line. Brightness variations at all photospheric levels were of an oscillatory nature with an interval of 1–5 min. The observed temporal variations of Fraunhofer line intensities in the spectra of the studied AR section suggest that the emergence of the new magnetic flux induced consecutive magnetic reconnections in the EB-1 region, the excitation propagated along a magnetic loop and initiated the formation of EB-2, and the two bombs then evolved as a physically connected pair.

Keywords: Sun, photosphere, activity, spectral study, Ellerman bombs

DOI: 10.3103/S0884591318020071

INTRODUCTION

Ellerman bombs (EBs) are one of the most intriguing manifestations of solar activity. The first H_α spectra of EBs were obtained in the process of visual and photographic solar observations performed by Walter Mitchell in 1909 (at Haverford College) and Ferdinand Ellerman in 1915 (at the Mount Wilson Observatory) [10]. The spectral appearance of these phenomena earned them another name: moustaches [6]. The most striking feature of EB spectra is bright narrow emission bands (up to 0.5 nm in width) in both wings of chromospheric lines and strong absorption at their center.

The morphology of EBs was characterized in [13, 14, 23, 26, 27, 40]. They are short-lived small-scale bright structures in the solar atmosphere (dots). Observations showed that they emerge primarily in young evolving active regions (ARs) with a complex magnetic structure (in the areas of emerging magnetic flux and in the vicinity of solar spots). It was found that their typical size and average lifetime are ~1″ and ~15 min. EBs are often accompanied by small-scale chromospheric ejections (surges), which are thought to be associated with magnetic reconnections in the lower chromosphere [13, 24, 41]. EBs are observed most often in the H_α line, but they are also seen as bright dots in the UV continuum near $\lambda = 160$ and 170 nm, Ca II H and K lines, and in the Ca II λ 854.2 nm line. However, these lines reveal much fewer EBs than H_α does [8, 16, 17, 25, 29, 31, 34]. Diffuse brightening in Na I D and Mg I b has also been reported [33]. Observations demonstrated [41] that half of all Ellerman bombs emerge and vanish in pairs.

Owing to their dynamic and explosive nature and the fact that they may influence the complex dynamics of the upper solar atmosphere and contribute significantly to heating of the lower chromosphere, Ellerman bombs have been studied extensively in recent years [14, 26–28]. It was suggested that EBs form as a result of magnetic reconnections in the lower chromosphere or the photosphere [8, 10, 13, 14, 30, 38, 39]. Conclusive evidence of their influence on the outer atmosphere is lacking: they are not observed in He II

λ 30.4, Fe IX λ 17.1, and Fe XIVλ 21.1 nm lines [38]. It was found that EBs are associated with strong magnetic fields in intergranular lanes and the majority of them emerge at sites where positive and negative polarities are driven by horizontal photospheric flows [18, 28].

The majority of studies focused on the properties of EBs rely on data obtained in observations of chromospheric lines. It is typical for researchers examining and modeling the EB photosphere to consider just the Fe Iλ 630.25 nm line forming in the upper photospheric layer [8, 9, 28, 32, 38].

An increase in the intensity of this line cospatial with a magnetic field concentration in the photosphere was reported in [28]. It was found that brightenings of the wings of the H_α line profile, which are interpreted as EBs, are often spatially correlated with increases in intensity of the Fe I λ 630.25 nm line core [28]. The authors attributed this to the fact that the lower chromosphere and the upper photosphere produce the dominant contribution to the wings of the optically thick chromospheric H_α line [36]. It was concluded in [28] that cospatial intensity increases in the Fe I λ 630.25 nm line core and the wings of the H_α line occurring in small bipolar regions both in observations and in simulations provide evidence in favor of photospheric magnetic reconnections being the underlying causes of EBs.

The Ti II λ 655.957 nm absorption line forming in the lower photospheric layer was used in [24] to study the photospheric EB velocity field. Time curves of the line-of-sight velocity in the upper and lower photospheric regions in the AR section with an evolving EB were presented in [4]. It was also suggested that Ellerman bombs form as a result of consecutive noncontiguous magnetic reconnections in the lower chromosphere or the upper photosphere. The results reported in [16, 21, 29] validate this assumption.

The aim of the presents study is to examine the specifics of variation of Fraunhofer lines in the spectra of EBs in different photospheric layers by comparing them to Fraunhofer lines in the quiet photosphere spectrum and in an AR section without active structures. The results of spectrophotometric analysis of two Ellerman bombs (EB-1 and EB-2) observed in evolving AR NOAA 11024 on July 4, 2009, are presented below. The variation of intensities of photospheric lines in the spectra of EBs and their surroundings measured at different stages of EB evolution is determined and interpreted.

This study is a continuation of our earlier work [5] where the results of analysis of spectral H_α observations of these two EBs were reported.

OBSERVATIONAL DATA

The studied Ellerman bombs (EB-1 and EB-2) emerged and evolved in active region NOAA 11024 [5, 22]. At the time of observations (on July 4, 2009), this AR was located near the central meridian of the solar disk (S25E02 (–29, –449)). It rapidly became more and more active: new magnetic fluxes emerged at different AR sections, pores and spots formed, and the number of microflares increased [12, 37]. Simultaneous observations in several spectral regions were conducted by E.V. Khomenko with the THEMIS French–Italian 90-cm vacuum telescope (Instituto de Astrofisica de Canarias, Tenerife Island, Spain). The duration of these observations was 20 min: they started at 9^h30^m UT and ended at 9^h50^m UT. Interestingly, their start coincided with the initial stage of evolution of EB-2.

Figure 1 shows the H_α spectra obtained at $9^h42^m45^s$ UT (both EBs are seen clearly) and at $9^h49^m34^s$ UT (the end of observations; EB-2 is bright, while EB-1 is barely visible with faint emission remaining just in the red wing of H_α).

The Ellerman bombs formed in the region of one of the three magnetic fluxes that were emerging then [37]. The brightness of EB-1 decreased in the process of observations, while the brightness of EB-2 increased. The results of analysis of spectral H_α observations were reported in our earlier study [5]: the SOHO/MDI AR magnetogram obtained on July 4, 2009, the studied AR section, the spectrograph slit position. The specific features of H_α spectra measured at different time points were characterized. Temporal variations of intensity in the H_α wings at distances of ±0.1 and ±0.15 nm from the line center and the specifics of variation of line-of-sight velocities of the chromospheric material in the region of EBs and in the surrounding regions were studied. The obtained data suggest that these EBs had formed and evolved as a physically connected pair.

The spectral region of λ ≈ 630 nm (Fig. 2) was used to examine the variation of plasma parameters at different photospheric levels in the process of EBs evolution. This region was chosen for the reason that it contains lines forming in a wide altitude range: two strong Fraunhofer neutral iron lines Fe Iλ 630.15 and 630.25 nm and two weak lines Fe I λ 630.35 nm and Ti I λ 630.38 nm. These lines are denoted in the text as Fe-1, Fe-2, Fe-3, and Ti, respectively. The width of the studied spectral region is 0.55 nm. The central depths of profiles and the altitudes of formation of centers of these lines in the quiet photosphere at the solar disk center are as follows: $d_0 = 0.719$, 0.650, 0.045, and 0.072; h = 489, 381, 139, and 180 km, respec-

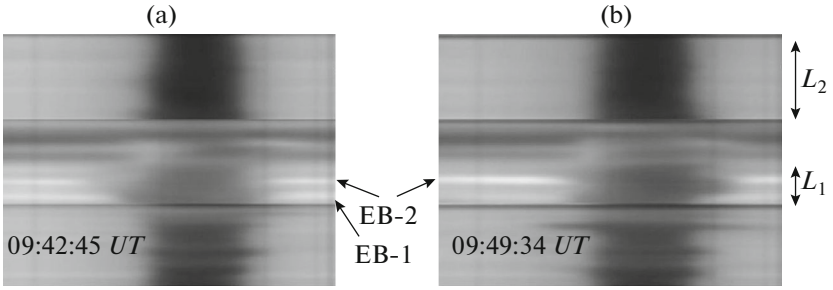

Fig. 1. H_α spectra of the AR obtained at different time points. EB-1 and EB-2 are Ellerman bombs, L_1 is the studied section, and L_2 is the AR section without active structures that lies outside the region of emerging magnetic flux.

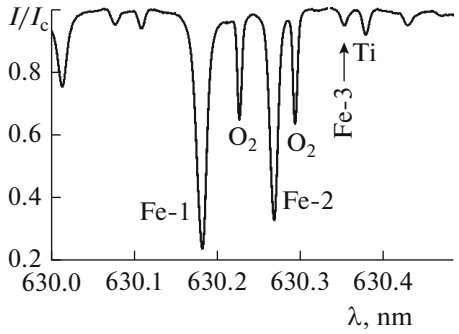

Fig. 2. Spectral region close to λ = 630 nm with the studied lines.

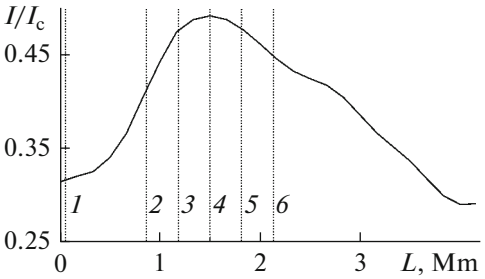

Fig. 3. Variation of the central intensity of Fe-1 along the spectrograph slit at $9^h34^m03^s$ UT. The spectral measurement sites are marked by vertical lines *1*–*6*.

tively [1]. The corresponding effective Landé g-factors are g_{eff} = 1.7, 2.5, 1.3, and 0.9 [7]. It can be seen that the first two lines are much deeper; therefore, it is reasonable to assume that weaker lines are produced at lower altitudes both in the quiet photosphere and in the active region. In other words, the central intensities of the first and the last two lines should form in the upper and the lower photospheric layers, respectively.

VARIATIONS OF PHOTOSPHERIC LINES IN THE SPECTRA OF ELLERMAN BOMBS AND THEIR VICINITY

Shape of Profiles. The Stokes *I* profiles obtained at different distances from the center of EB-1 (with 160-km-long intervals) were studied. Figure 3 shows the distribution of the central intensity of Fe-1 along the spectrograph slit obtained at $9^h34^m03^s$ UT with indicated measurement sites and their numbers. The shape variation of profiles of photospheric lines in the spectra of Ellerman bombs and their vicinity and in the spectra measured at different stages of EB evolution is analyzed below.

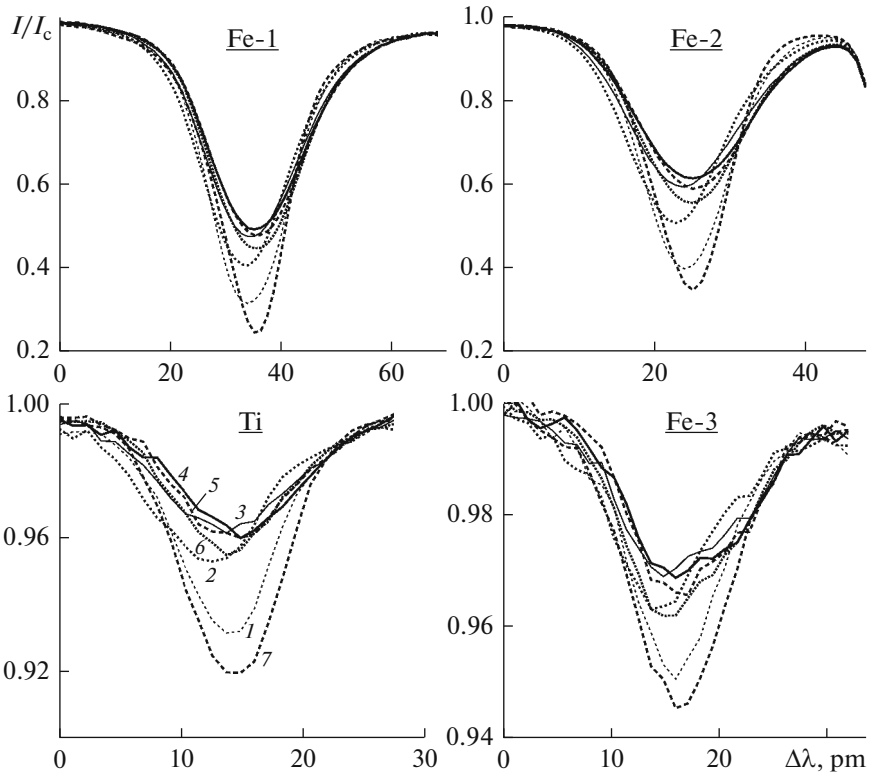

Fig. 4. Profiles of Fraunhofer lines in the EB-1 spectra obtained for different distances from the center of this Ellerman bomb (sites *1*–*6* in Fig. 3) at $9^h34^m03^s$ UT. Profiles *7* were obtained for the AR section without active structures that lies outside the region of emerging magnetic flux.

Figure 4 presents the profiles of lines in the EB-1 spectra at different distances from the center of this Ellerman bomb. These spectra were obtained at $9^h34^m03^s$ UT (3 min after the start of observations). It will be demonstrated below (Figs. 10, 11) that the brightness of EB-1 increased sharply at this point in time, while EB-2 was at the earliest stages of its evolution. It follows from Fig. 3 that profiles *1* were obtained outside the EB-1 area; profiles *4* corresponded to the EB center; and profiles *3*, *5* and *2*, *6* were obtained for distances of ±0.33 and ±0.67 Mm from the EB center, respectively. Profiles *7* obtained in an AR section without active structures outside the region of emerging magnetic flux (L_2 in Fig. 1) are shown for comparison. The central depth of these profiles differs from that of line profiles for the quiet photosphere by 4% (Fe-1 line) or less than 1% (the other lines).

It can be seen that the profiles of lines forming in the upper photospheric layer (Fe-1 and Fe-2) are smooth and asymmetric; their central intensity increases from the edges to the center of the EB. Residual intensity I/I_c in the spectrum of the central part of the Ellerman bomb (profile *4*) is 18 and 22% higher than I/I_c in the surrounding photosphere (profile *1*) for Fe-1 and Fe-2, respectively. The short-wave wings and the central parts of profiles *1* and *2* are blueshifted relative to profile *7*. The central part of profile *3* is blueshifted, while the red wing is redshifted (red asymmetry). Profile *4* for the EB center and profiles *5* and *6* are redshifted relative to profile *7* and feature red asymmetry in their wings. Thus, profiles obtained for the same distance from the EB center (±0.33 and ±0.67 Mm) are shifted in opposite directions relative to profile *7*, but all of them feature red asymmetry in their wings. This is probably associated with the upward and downward motion of photospheric material.

It is interesting to note the variation of intensity in the red wing of line Fe-2: when the residual intensity increased at the center of the line, I/I_c in the red wing decreased, while the variation of I/I_c in the blue wing was within the limits of measurement error.

It is evident that the asymmetry of profiles of Fraunhofer lines forming in the lower photospheric layers (Fe-3 and Ti) is more pronounced. Just as in the upper photosphere, profiles *1* and *7* are smooth. The intensity of profile *1* is ~1% higher than that of profile *7*. The central intensity of Fe-3 and Ti profiles at the EB center is 3 and 2% higher that the central intensity of the corresponding profiles in the surrounding

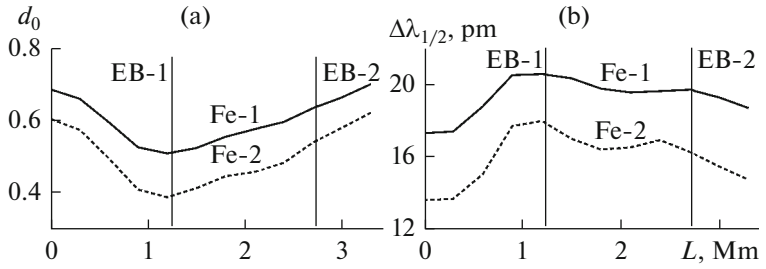

Fig. 5. Variation of (a) central depth d_0 and (b) FWHM $\Delta\lambda_{1/2}$ of Fe-1 and Fe-2 profiles over the studied AR section. Vertical lines mark the EB centers.

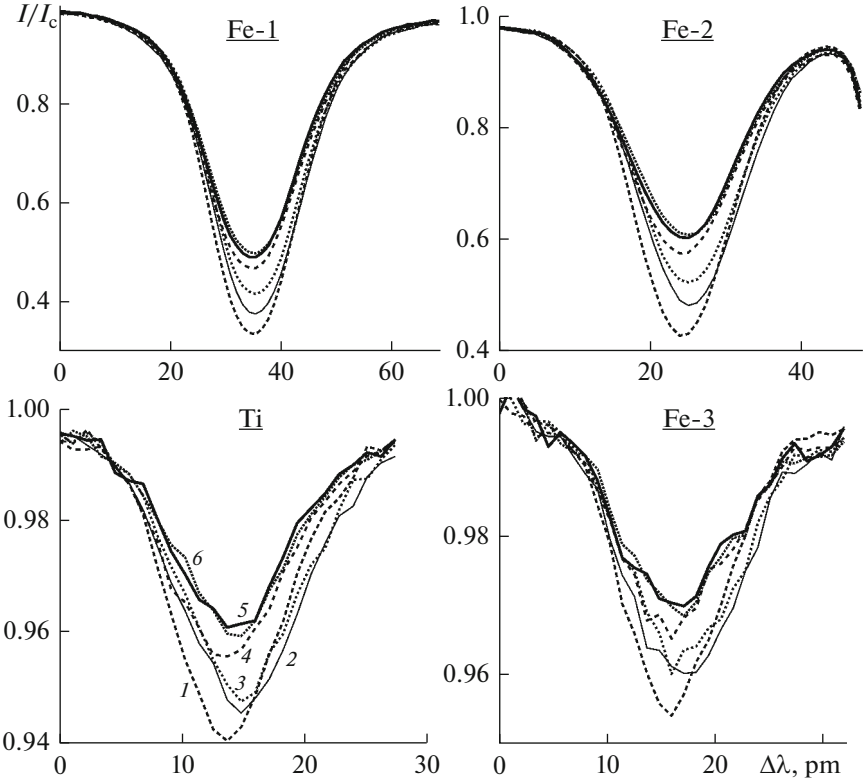

Fig. 6. Profiles of Fraunhofer lines in the spectra for the central part of EB-2 obtained at different stages of its evolution. Curves *1–6* correspond to the following time points: $9^h31^m07^s$, $9^h35^m32^s$, $9^h38^m07^s$, $9^h44^m42^s$, $9^h47^m40^s$, and $9^h48^m20^s$ UT.

photosphere. The asymmetry of Fe-3 profiles is more pronounced: the majority of them contain several components concentrated in the long-wave wing. The short-wave wing is smoother, but discernible components were also occasionally observed in it. Components were often found in both wings of profiles obtained for the central EB part. This suggests that the lower EB photosphere layers had a finer structure; i.e., they were formed by several plasma jets with different temperatures and velocities.

The FWHM of profiles also varied. It was found that FWHM $\Delta\lambda_{1/2}$ of line profiles increased with a reduction in their central depth d_0. Figure 5 presents the variation of these quantities over the studied AR section for lines Fe-1 and Fe-2 (vertical lines denote the EB centers). It can be seen that d_0 and $\Delta\lambda_{1/2}$ varied in the antiphase.

The temporal variation of shape of profiles of Fraunhofer lines at the center of EB-2 in spectra obtained at different stages of its evolution is presented in Fig. 6. It should be recalled that the start of observations coincided with the onset of evolution of EB-2; i.e., the first spectra correspond to its earliest stages. We have determined in [5] that the H_α wings intensity in the spectra in the EB-2 region started

increasing when the observations commenced; 5 min (after $9^h35^m32^s$ UT), a well-defined maximum (corresponding to the evolving EB-2) in the H_α wings emerged in the curve of intensity variation along the spectrograph slit. At the end of observations, EB-2 was brighter than EB-1.

Figure 6 shows the temporal variation of profiles of lines forming in different photospheric layers. Profiles *1* for the central part of EB-2 correspond to one of the first spectra. Their intensity I/I_c is 5 and 8% higher than that of quiet-photosphere profiles of lines forming in the upper photospheric layer (Fe-1 and Fe-2) and 1% higher than I/I_c of quiet-photosphere profiles of lines forming in the lower layer (Fe-3 and Ti). All profiles are smooth. Profiles *2–6* correspond to different observational time points (see the caption of Fig. 6). Profiles 2 were obtained at $9^h35^m32^s$ UT and had a distinct red asymmetry, while the blue wing of the H_α line was the more intense one at the time [5]. Their central parts are redshifted relative to profiles *1*. The profile intensity increased by 4 and 6% for Fe-1 and Fe-2 and by 1% for Fe-3 and Ti; $\Delta\lambda_{1/2}$ increased by 3, 7, 14, and 23% for Fe-1, Fe-2, Ti, and Fe-3, respectively. It is evident that the profiles of lines forming in the lower photospheric layer have broadened considerably relative to profile *1*. This suggests that the motion of material in this region became more vigorous. It was concluded in [6] that the Doppler contour of metal lines in EB spectra is defined almost exclusively by the velocities of turbulence-like macroscopic motions.

The residual intensity of profiles in the EB-2 spectra generally increased until the end of observations. The profiles are asymmetric, and this asymmetry is more pronounced for the Fe-3 line that forms in the lower photospheric layer. It should be noted that the I/I_c and $\Delta\lambda_{1/2}$ values increased nonuniformly with time: the intensity and the FWHM of all profiles *3* were higher than the corresponding values obtained at a later point in time (2 min later).

Figure 6 also demonstrates that the maximum I/I_c values were obtained toward the end of observations at $9^h47^m40^s$ UT for Fe-1 and Fe-2 and at $9^h48^m20^s$ UT (i.e., 40 s later) for Ti and Fe-3. It is likely that excitation propagated from the upper photospheric layers to the lower ones. The central intensities and the FWHM values of profiles of Fe-1, Fe-2, Ti, and Fe-3 determined at these time points were 22, 26, 3, and 2% and 40, 47, 15, and 33% higher than the corresponding values in the unperturbed photosphere, respectively.

The calculation results demonstrate that the shape of the Fe I λ 630.25 nm line profile underwent the most significant changes.

Similar shape variations of profiles of Fraunhofer lines in the spectrum of an Ellerman bomb were reported in [2]. It was found that the profile of the Fe I λ 630.25 nm line at the center of the studied EB is 18–23% weaker (and has a 40–70% larger FWHM value) than the profile in the unperturbed photosphere.

Intensity Variations. It is known that the primary factors influencing all active processes in the photosphere are granulation (induced by convective motion) and quasiperiodic 5-min intensity and velocity variations (driven by wave motion). The intensity and velocity variations induced by convection were characterized in detail in [3] through statistical analysis of observational data in the range from the continuum formation level to the temperature minimum. The relation between 5-min intensity and velocity variations and granulation was also studied in the quiet solar photosphere for the Fe I λ 532.4185 nm line.

The AR section examined in the present work was located in the region of emerging magnetic flux and evolving EBs (L_1 in Fig. 1). In order to reveal changes in the physical state of photospheric material induced by Ellerman bombs, we also studied an AR section without active structures that lies outside the region of emerging magnetic fluxes (L_2 in Fig. 1). The spectra of these sections were observed at one and the same time. Figures 7a and 7b show the variation of intensity (in arbitrary units) along the spectrograph slit at the continuum formation level in the spectra of L_2 and L_1 at different points in time. Section L_2' is located within L_2 and has the same length as L_1. Curves *1* and *6* correspond to the very start of observations and one of the last observational time points. Granules and intergranular lanes are seen clearly; it is also evident that the granulation pattern changed with time (as in the quiet photosphere [3]) in the course of 20-min-long observations. Granules and intergranular lanes were involved in horizontal motion, and the area occupied by them in section L_1 was smaller than that in section L_2'. The maximum amplitude of intensity variations was approximately 10 and 13% in L_1 and L_2', respectively. The central EB parts were located in intergranular lanes. In the process of observations, the intensity increased throughout the entire section L_1, but the granule and intergranule intensity values in the region of formation of EB-1 were larger than the corresponding values in the EB-2 region. The difference between intergranule intensities in the regions of EB-1 and EB-2 was as large as 10% (curve *2*). It should be noted that the intensity of the EB-2 intergran-

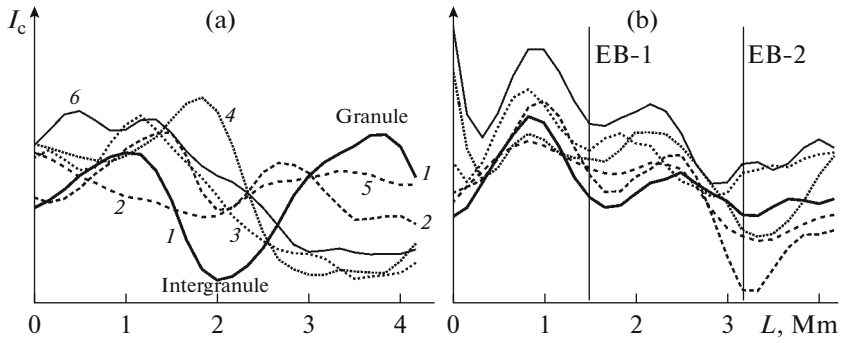

Fig. 7. Variations of intensity along the spectrograph slit at the continuum formation level in the spectra of (a) the AR section without active structures that lies outside the region of emerging magnetic flux (curves *1*–*6* correspond to the following time points: $9^h30^m56^s$, $9^h35^m57^s$, $9^h39^m06^s$, $9^h44^m42^s$, $9^h47^m21^s$, and $9^h48^m20^s$ UT); (b) the AR section with evolving EBs (observational time points remain the same). Vertical lines mark the EB centers.

ular lane decreased considerably (by 8%; see curves *1* and *2*) at the initial stage of observations, but then increased gradually. A granule started forming at this site toward the end of observations.

The obtained data corroborate the assertion [15] that the evolution of emerging magnetic flux at the photospheric level is characterized by distortion of the granulation pattern.

Figure 8 shows the variation of residual intensities at the centers of the studied photospheric lines in the spectrum of L_2. The variations of intensity in a granule and the adjacent intergranular lane (regions above these granule and intergranular lane) were examined for lines forming in the lower (upper) photospheric layer. It can be seen that the granule intensity at the continuum formation level is 15% higher than the intergranule intensity. The ratio of granule and intergranule intensities at the altitudes of formation of the studied photospheric lines changed several times in the process of observations. In certain time intervals (e.g., from $9^h36^m26^s$ to $9^h37^m54^s$ UT), the granule was brighter than the intergranular lane throughout the entire height of the photosphere.

Quasiperiodic intensity variations are seen clearly. In the region of formation of the Fe-1 line, they occurred in 5-min intervals, and the central depth was 3% lower (on average) than the one in the quiet photosphere. In the regions of formation of other lines (Fe-2, Fe-3, and Ti), the interval was ~3–5 min, and the central depth was reduced by 1% compared to the quiet photosphere. The average amplitude of I/I_c variation at the center of Fe-1 above the intergranular lane and above the granule is 8 and 5%, respectively. This agrees with the findings made in [3]. The authors of [3] have investigated the intensity variations at the center of the Fe I λ 532.4185 nm line that forms, just as the Fe Iλ 630.25 nm (Fe-1) line, in the upper photosphere. It was concluded in this study that stronger intensity variations occur above intergranular lanes. It follows from Fig. 8 that the amplitudes of I/I_c variation above the intergranular lane and above the granule in the region of formation of Fe-2 are approximately the same (6–8%). The amplitude of I/I_c variation in the lower photospheric layer (where lines Ti and Fe-3 form) above the granule is 2% and is larger than the corresponding amplitude above the intergranular lane (1%).

The central intensities of Fraunhofer lines in the spectra of EB regions and their surroundings were determined at different stages of EBs evolution.

Figure 9 presents the intensity variations along the spectrograph slit at the centers of the studied photospheric lines at different time points. Curves *1* and *5* correspond to the start and the end of observations. It can be seen that curves *1* have a clear maximum corresponding to EB-1 at all levels of the photosphere and show signs of an intensity increase in the right wing. At subsequent time points, the intensity increase spreads along the AR; curves *2* and *3* feature a distinct maximum corresponding to the evolving EB-2. It is evident that EB-1 was brighter than EB-2 at the time, but it faded gradually, while the brightness of EB-2 increased with time. Curves *4* correspond to the moment when the brightness of EB-1 and EB-2 were roughly equal. At the end of observations, EB-2 was brighter than EB-1 (curves *5*).

Intensity curves *3* for Fe-1 obtained 7 min after the start the observations have a well-marked maximum corresponding to the evolving EB-2. The brightness of EB-1 was 5% higher than that of EB-2 at the time, and the distance between the EB centers in this photospheric region was $L = 1.25$ Mm. This distance increased gradually to 1.67 Mm at $9^h42^m03^s$ UT (~12 min after the start observations) and remained unchanged at later times. Curve *5* shows that the brightness of EB-2 was 6% higher than that of EB-2 at

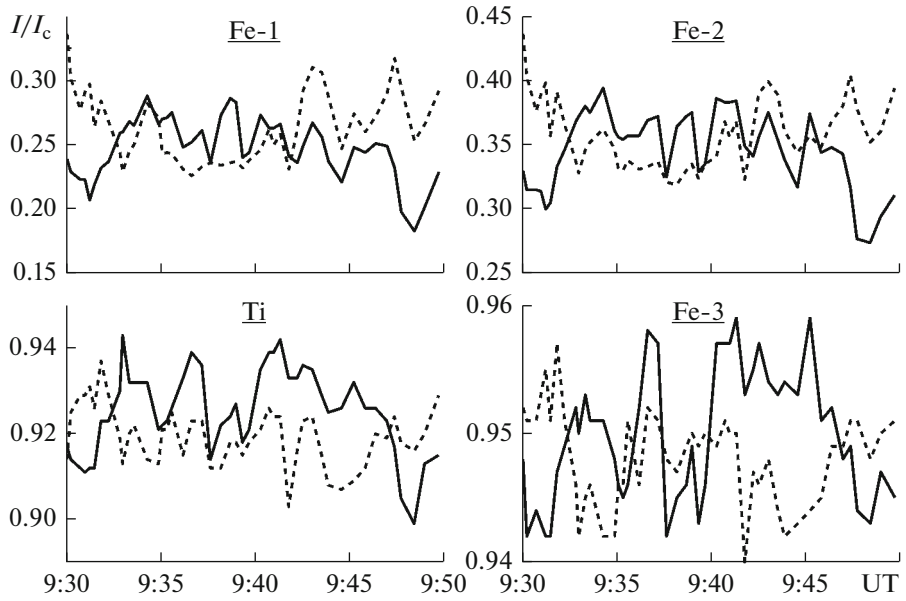

Fig. 8. Temporal variation of the central intensities of Fraunhofer lines in the spectra of section L_2. Solid curves correspond to the granule and the region above it; dashed curves correspond to the intergranular lane and the region above it.

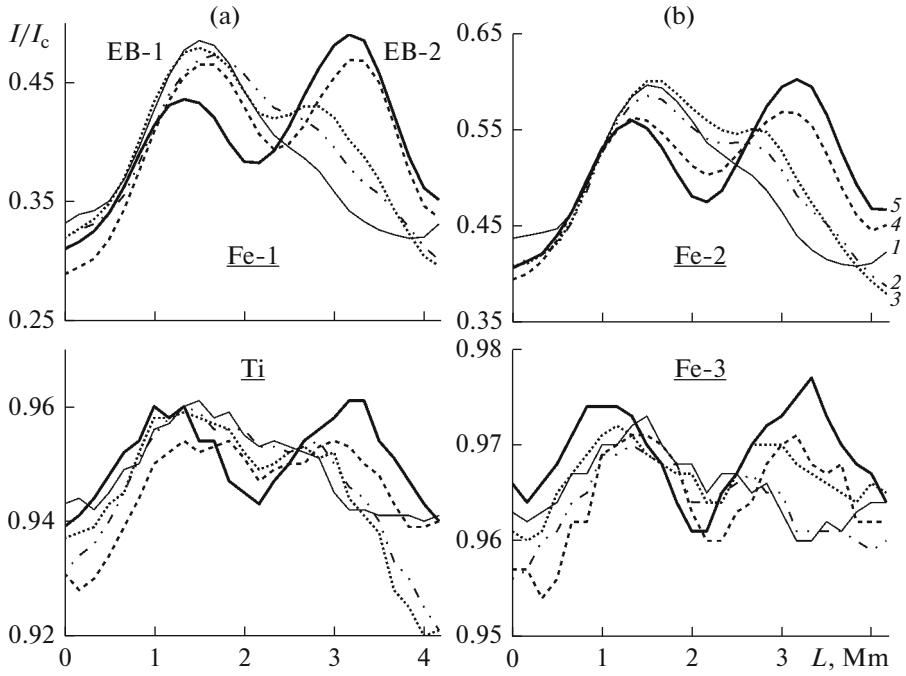

Fig. 9. Variation of the central intensities of photospheric lines along the spectrograph slit at different time points. Curves *1* correspond to $9^h30^m56^s$ UT; curves *5* correspond to $9^h48^m20^s$ UT; curves *2–4* correspond to $9^h35^m57^s$, $9^h37^m11^s$, and $9^h44^m42^s$ (for Fe-1); $9^h35^m42^s$, $9^h36^m11^s$, and $9^h45^m18^s$ (for Fe-2); $9^h35^m57^s$, $9^h37^m11^s$, and $9^h42^m45^s$ (for Ti); $9^h34^m17^s$, $9^h39^m43^s$, and $9^h42^m28^s$ UT (for Fe-3).

the end of observations. The curves of I/I_c variation for Fe-2 are similar, but the distance between the EB centers in this photospheric region increased to 1.83 Mm, and EB-2 was 5% brighter than EB-1 at the end of observations.

It can be seen that the brightness variation in the lower photospheric layer (lines Ti and Fe-3) had a finer structure. Apparently, the material flow at this level of the photosphere consisted of several jets with

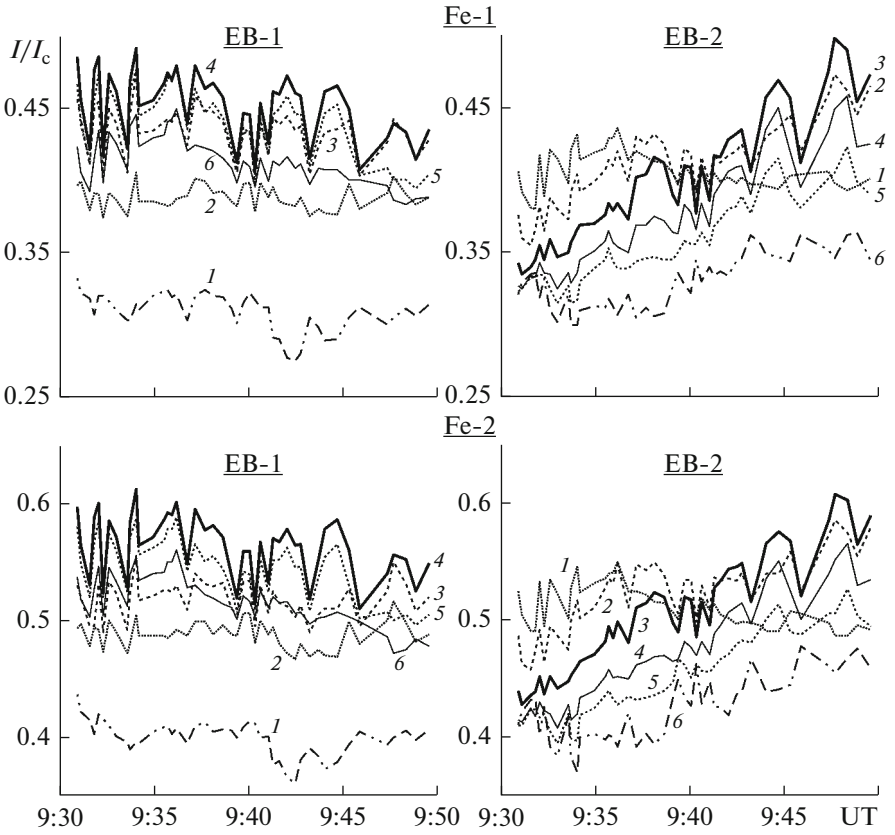

Fig. 10. Temporal variation of intensities of photospheric lines Fe-1 and Fe-2 at different distances from the centers of EB-1 and EB-2 in the upper photospheric layer.

different temperatures and velocities. The central intensity of Ti and Fe-3 in the EB-1 spectra decreased only by 0.5% (and increased by 2–3% in the EB-2 spectra) in the course of observations. The brightness of EB-1 and EB-2 differed by no more than 1% at the end of observations. The distance between these Ellerman bombs increased to 2.1 and 2.3 Mm at the level of formation of Ti and Fe-3, respectively.

The patterns of EB intensity variation along the spectrograph slit were generally very similar in our observations at different photospheric levels. However, the time points of equalization of brightness of two EB and the emergence of a well-marked intensity maximum corresponding to EB-2 differed. The distance between the EBs became shorter with photospheric altitude. The area occupied by the Ellerman bombs also varied and reached its maximum in the lower photospheric layer at the end of observations.

Figures 10 and 11 show the temporal variation of intensities at the centers of the studied photospheric lines in the spectra of EB-1, EB-2, and their surroundings. Thick solid curves *4* and *3* correspond to the central parts of EB-1 and EB-2. Curves *1* (EB-1) and *6* (EB-2) were plotted based on the spectra measured outside the EBs (in their vicinity). Curves *3*, *5* and *2*, *6* for EB-1 and curves *2*, *4* and *1*, *5* for EB-2 correspond to regions located at distances of ±0.33 and ±0.66 Mm from the centers of Ellerman bombs. Figure 10 illustrates the I/I_c variation in the upper photospheric layer, and Fig. 11 presents the data for the lower layer.

It can be seen that the brightness of EB-1 decreased in the course of observations, while EB-2 became brighter with time. Brightness variations at all photospheric levels were of an oscillatory nature with an interval of 1–5 min. It was noted in [19] that the evolution curves of "moustaches" have the shape of a sequence of peaks. The central intensities of lines increased from the EB edges to their central part. The amplitude of brightness variations also increased toward the EB centers (and increased with time for EB-2). The variations of time curves of intensity were synchronized in the regions of EB evolution, but this synchronicity subsided at the boundaries of these regions. The intensity in AR sections lying outside the EBs (in their vicinity) varied in the antiphase.

Three distinct peaks (with 1-min intervals between them) at 9^h32^m, 9^h33^m, and 9^h34^m are seen in all EB-1 brightness curves measured in different photospheric layers within the first 3 min of observations.

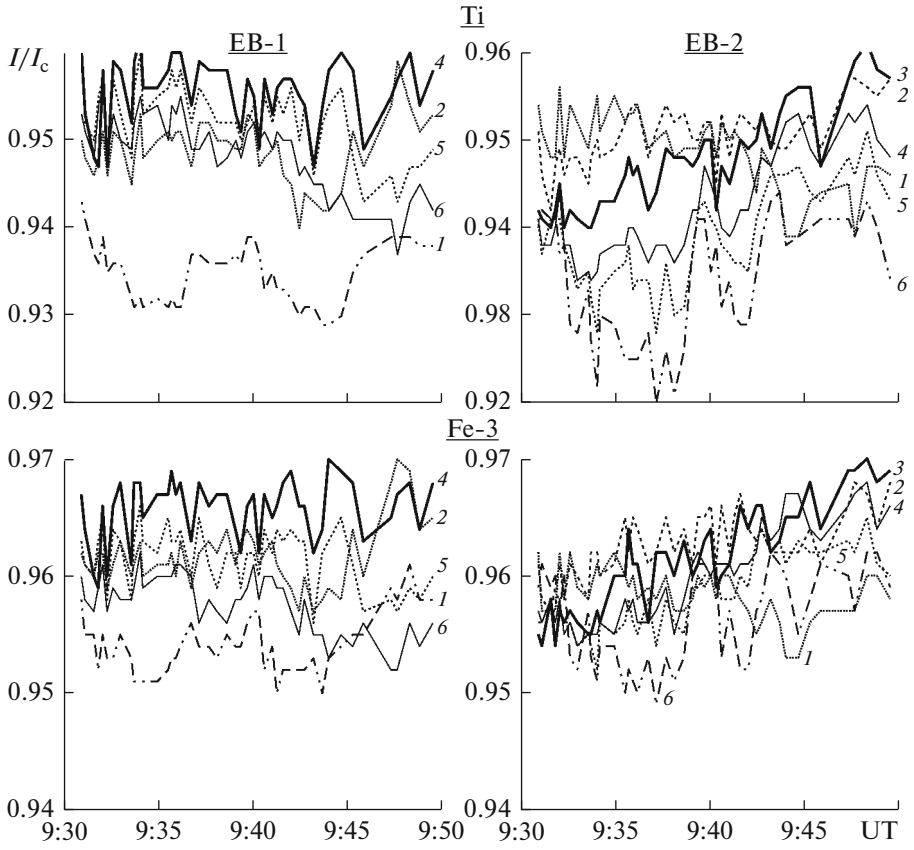

Fig. 11. Same for the lower photospheric layer (lines Ti and Fe-3).

These peaks agree well with the intensity peaks in the wings of H_α (see Fig. 6a in [5]) and are indicative of pulsed energy discharges resulting from successive magnetic reconnections. It was found in [5] that the intensity increase in the wings of H_α was not associated with any changes in the central intensity of this line (EB-1) or coincided with a certain reduction in this central intensity (EB-2). This suggests that magnetic reconnections occurred well below the chromospheric layer in which the core of H_α forms.

The excitation caused by the impulse release of energy in the region of EB-1 started propagating along the AR (along the magnetic loop) and gave rise to EB-2. The gradual increase in the residual intensity of lines in the EB-2 spectra is seen in Figs. 10 and 11. It is known that EB pairs often emerge at the footpoints of compact magnetic loops. The intensity variation curves show that the I/I_c values in the intensity peaks were the highest at the center of EB-1. These peaks (although with a lower amplitude) are visible in curves *5*, *6* for EB-1 and *1*, *2* for EB-2. The propagation of the region of increased intensity, which corresponds to the evolving EB-2, along the AR is also seen clearly in Figs. 9 and 12a. The results reported in [20, 21, 28, 39, 40] corroborate the assertion that EBs form as a result of successive intermittent magnetic reconnections in the lower chromosphere or the upper photosphere. It was suggested in [30] that individual pulses observed in the UV range in the process of EB evolution may be associated with pulsed reconnections. It was found in [16] that magnetic reconnections in an Ellerman bomb are successive and periodic.

It should be noted that the intensity variation curves for the upper photosphere in the spectrum of the central part of EB-2 agree well with the curve of intensity variation in the red wing of H_α, while similar curves for EB-1 agree with the variation of intensity in the blue wing of H_α (the well-marked peak at $9^h40^m04^s$ UT in the red wing of H_α is weak at the photosphere level).

The pattern of EB-1 brightness variation in the upper and the lower photospheric layers is the same. Figure 11 shows that the curves of intensity variation for EB-2 had a finer structure in the lower photospheric layer.

The changes in the central intensity of lines in the spectra of EBs and their surroundings differed in magnitude. The residual intensity of lines Fe-1, Fe-2, Ti, and Fe-3 in the spectra of central parts of EB-1 and EB-2 changed by 15, 18, 3, and 2% and 13, 12, 2, and 1%, respectively, relative to the corresponding

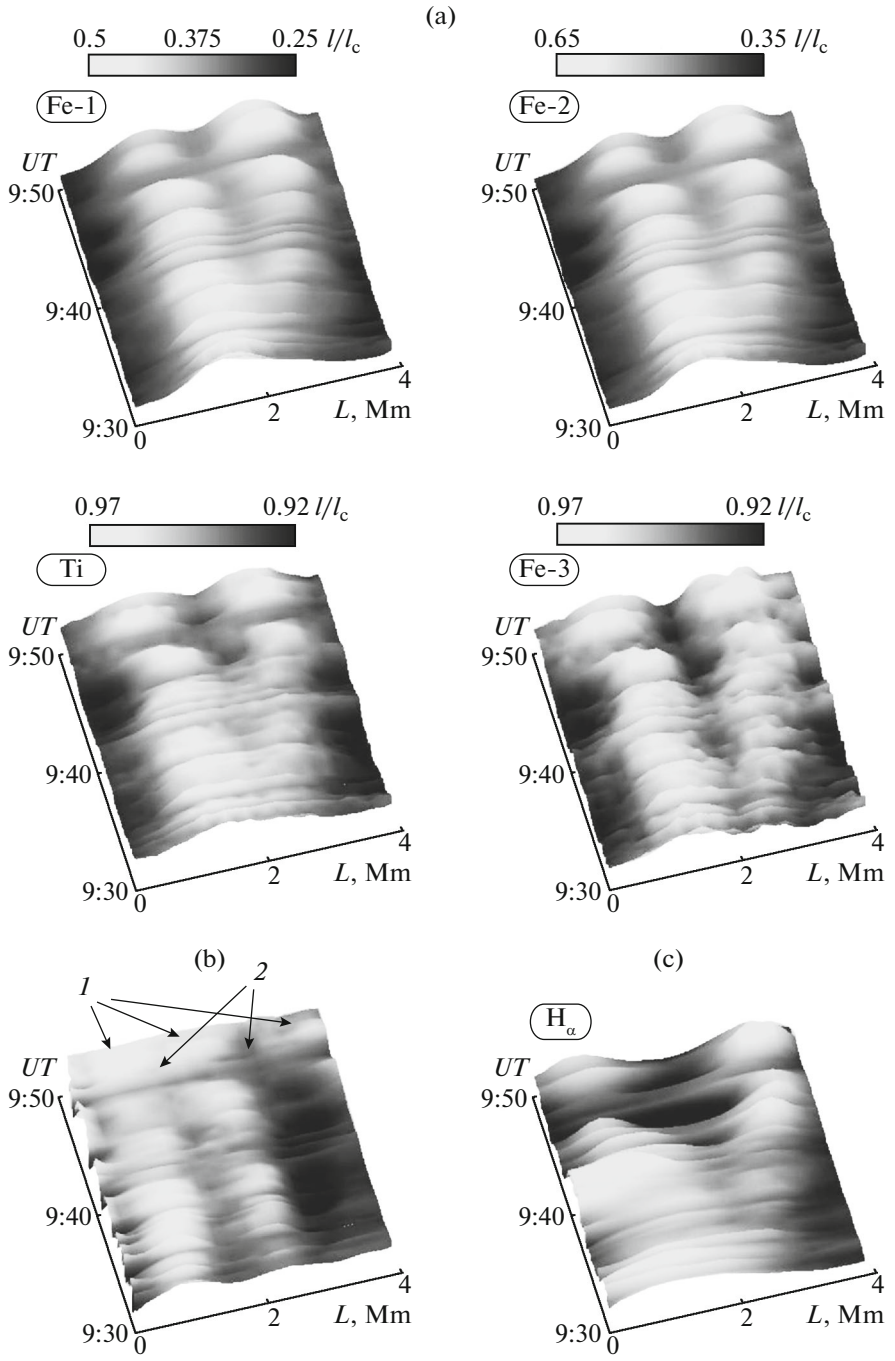

Fig. 12. Temporal variation of intensity along the spectrograph slit (a) at different photospheric levels; (b) at the continuum formation level (arbitrary units; *1* and *2* denote granules and intergranular lanes); (c) in the red wing of the H_α line (in arbitrary units).

intensity in the spectra of EB surroundings. It is evident that the lower photospheric layer was hardly affected by the excitation that gave rise to EB-2.

Figure 12 represents the variations of intensity along the spectrograph slit at different photospheric levels (from the continuum formation region to the upper layers). The corresponding pattern for H_α is also shown for comparison.

Figure 12a shows clearly that the temporal variations of intensity were of an oscillatory nature and had a finer structure in the lower photospheric layer. The intensity variation at the continuum formation level

is shown in Fig. 12b. The changes in the granulation pattern occurring in the course of observations are evident. Arrows and numbers *1* and *2* denote the granule and intergranule regions, respectively. It follows from the comparison of Figs. 12a and 12b that Ellerman bombs formed in intergranular lanes. It was hypothesized in [18] that the emergence of Ellerman bombs may be associated with strong magnetic fields in intergranular lanes. Figure 12a provides a clear illustration of propagation of the excitation from the region of EB-1 along the AR and the resulting development of EB-2 in the adjacent intergranular lane. It should be noted that the intensity in this intergranular lane decreased considerably in the process; by the end of observations, the intensity increased, and a new granule emerged near the intergranule. Figure 12a also demonstrates that the brightness variations in the regions of EB evolution were synchronized. In other words, these EBs evolved as a physically connected pair.

Figure 12c presents the temporal variations of intensity along the spectrograph slit in the red wing of the H_α line at a distance of 0.1 nm from its center. It follows from the comparison of Figs. 12c and 12a that the increases in intensity in the cores of all the studied photospheric lines and in the wings of H_α are correlated spatially.

CONCLUSIONS

The results of analysis of spectral observations of two Ellerman bombs EB-1 and EB-2, which were formed and have evolved in the area of emerging magnetic flux in active region NOAA 11024, were presented. The brightness of EB-1 decreased in the process of observations, while the brightness of EB-2 increased. The spectral region of $\lambda \approx 630$ nm with photospheric lines forming in a wide altitude range was examined. The variation of central intensities of Fraunhofer lines in the spectra of EBs and their vicinity at different stages of EB evolution and at different photospheric levels (from the continuum formation region to the upper layers) was analyzed.

The Stokes *I* profiles spaced by intervals corresponding to a distance of 160 km on the solar surface were studied. The most significant changes of the profile shape were observed for the Fe Iλ 630.25 nm line (the most magnetosensitive of all the studied lines). Its central depth and FWHM in the spectrum of the EB-2 center were 50% smaller and 30% larger than the corresponding values in the quiet photosphere. It was also found that the profiles of metal lines determined at different stages of EB evolution were asymmetric. This asymmetry was more pronounced in weak lines with their profiles containing several discernible components. This suggests that the EBs had a fine structure, and the material flow in the lower photospheric layer consisted of several jets with different temperatures and velocities.

It was found that the Ellerman bombs formed in intergranular lanes. The granulation pattern in the EBs region was altered compared to the pattern in the AR section without active structures that lies outside the region of emerging magnetic flux.

The distance between the EBs became shorter with photospheric altitude. The area occupied by the Ellerman bombs also varied and reached its maximum in the lower photospheric layer at the end of observations.

An increase in the core intensity of all the studied photospheric lines was correlated spatially with an increase in the wings intensity of the H_α line.

Brightness variations in the process of EBs evolution were of an oscillatory nature at all photospheric levels with an interval of 1–5 min.

The observed temporal variations of Fraunhofer line intensities in the spectra of the studied AR section in the regions of EBs and in their surroundings suggest that the excitation induced by consecutive magnetic reconnections in the EB-1 region propagated along a magnetic loop and initiated the formation of EB-2, and the two bombs then evolved as a physically connected pair.

ACKNOWLEDGMENTS

I thank E.V. Khomenko, R.I. Kostyk, and I.E. Vasil'eva for providing the THEMIS observational data and processing software.

REFERENCES

1. E. A. Gurtovenko and R. I. Kostyk, *Fraunhofer Spectrum and a Solar Force System for Oscillators* (Naukova Dumka, Kiev, 1989) [in Russian].
2. N. N. Kondrashova, "Spectropolarimetric investigation of an Ellerman bomb: 1. Observations," Kinematics Phys. Celestial Bodies **32**, 13–22 (2016).

3. R. I. Kostyk and N. G. Shchukina, "Five-minute oscillations and the fine structure of the solar photosphere. I," Kinematika Fiz. Nebesnykh Tel **15**, 25–37 (1999).
4. M. N. Pasechnik, "Plasma motions in the solar loop of emerging magnetic flux," Kinematics Phys. Celestial Bodies **30**, 161–172 (2014).
5. M. N. Pasechnik, "Spectral study of a pair of Ellerman bombs," Kinematics Phys. Celestial Bodies **32**, 55–69 (2016).
6. A. B. Severnyi, "Investigation of the fine structure of the emission of active formations and nonstationary processes on the Sun," Izv. Krym. Astrofiz. Obs. **17**, 129–161 (1957).
7. J. M. Beckers, *A Table of Zeeman Multiplets* (Air Force Cambridge Research Laboratories, Bedford, MA, 1969), in Ser.: *Physical Science Research Papers*, Vol. 371.
8. A. Berlicki, P. Heinzel, and E. H. Avrett, "Photometric analysis of Ellerman bombs," Mem. Soc. Astron. Ital. **81**, 646–652 (2010).
9. L. Bharti, Th. Rimmele, R. Jain, et al., "Detection of opposite polarities in a sunspot light bridge: evidence of low-altitude magnetic reconnection," Mon. Not. R. Astron. Soc. **37**, 1291–1295 (2007).
10. M. D. Ding, J.-C. Henoux and C. Fang, "Line profiles in moustaches produced by an impacting energetic particle beam," Astron. Astrophys. **332**, 761–766 (1998).
11. F. Ellerman, "Solar hydrogen "bombs"," Astrophys. J. **46**, 298–301 (1917).
12. A. J. Engell, M. Siarkowski, M. Gryciuk, et al., "Flares and their underlying magnetic complexity," Astrophys. J. **726**, 12–20 (2011).
13. C. Fang, Y. H. Tang, Z. Xu, et al., "Spectral analysis of Ellerman bombs," Astrophys. J. **643**, 1325–1336 (2006).
14. M. K. Georgoulis, D. M. Rust, P. N. Bernasconi, et al., "Statistics, morphology, and energetics of Ellerman Bomb," Astrophys. J. **575**, 506–528 (2002).
15. S. L. Guglielmino, L. R. Bellot Rubio, F. Zuccarello, et al., "Multiwavelength observations of small-scale reconnection events triggered by magnetic flux emergence in the solar atmosphere," Astrophys. J. **724**, 1083–1098 (2010).
16. Y. Hashimoto, R. Kitai, K. Ichimoto, et al., "Internal fine structure of Ellerman bombs," Pubis Astron. Soc. Jpn. **62**, 879–891 (2010).
17. M. Herlender and A. Berlicki, "Multi-wavelength analysis of Ellerman bomb light curves," Cent. Eur. Astrophys. Bull. **35**, 181–186 (2011).
18. D. B. Jess, M. Mathioudakis, P. K. Browning, et al., "Microflare activity driven by forced magnetic reconnection," Astrophys. J. Lett. **712**, L111–L115 (2010).
19. L. K. Kashapova, "A spectropolarimetric study of Ellerman bombs," Astron. Rep. **46**, 918–924 (2002).
20. R. Kitai, "On the mass motions and the atmospheric states of moustaches," Sol. Phys. **87**, 135–154 (1983).
21. R. Kitai, "Ellerman bomb as a manifestation of chromospheric fine scale activity," in *Proc. 5th Hinode Science Meeting, Cambridge, MA, Oct. 10–15, 2011* (Astronomical Society of the Pacific, San Francisco, CA, 2012), in Ser.: ASP Conference Series, Vol. 456, p. 81.
22. N. N. Kondrashova, M. N. Pasechnik, S. N. Chornogor, et al., "Atmosphere dynamics of the active region NOAA 11024," Sol. Phys. **284**, 499–513 (2013).
23. H. Kurokawa, I. Kawaguchi, Y. Funakoshi, et al., "Morphological and evolutional features of Ellerman bombs," Sol. Phys. **79**, 77–84 (1982).
24. T. Matsumoto, R. Kitai, K. Shibata, et al., "Height dependence of gas flows in an Ellerman bomb," Pubis Astron. Soc. Jpn. **60**, 95–102 (2008).
25. T. Matsumoto, R. Kitai, K. Shibata, et al., "Cooperative observation of Ellerman bombs between the Solar Optical Telescope aboard Hinode and Hida/Domeless Solar Telescope," Pubis Astron. Soc. Jpn. **60**, 577–584 (2008).
26. C. J. Nelson, J. G. Doyle, R. Erdélyi, et al., "Statistical analysis of small Ellerman bomb events," Sol. Phys. **283**, 307–323 (2013).
27. C. J. Nelson, E. M. Scullion, J. G. Doyle, et al., "Small-scale structuring of Ellerman bombs at the Solar Limb," Astrophys. J. **798**, 19 (2015).
28. C. J. Nelson, S. Shelyag, M. Masthioudakis, et al., "Ellerman bombs — Evidence for magnetic reconnection in the lower solar atmosphere," Astrophys. J. **779**, 125 (2013).
29. E. Pariat, B. Schmieder, A. Berlicki, et al., "Spectrophotometric analysis of Ellerman bombs in the CaII, Hα, and UV range," Astron. Astrophys. **473**, 279–289 (2007).
30. E. Pariat, B. Schmieder, A. Berlicki, et al., "Spectrophotometry of Ellerman bombs with THEMIS," in *Proc. The Physics of Chromospheric Plasmas, Coimbra, Portugal, Oct. 9–13, 2006*, Ed. by P. Heinzel, I. Dorotovi., and R. J. Rutten (Astronomical Society of the Pacific, San Francisco, CA, 2007), in Ser.: *ASP Conference Series*, Vol. 368, 253–258 (2007).
31. J. Qiu, M. D. Ding, H. Wang, et al., "Ultraviolet and Hα emission in Ellerman bombs," Astrophys. J. Lett. **544**, L157–L161 (2000).

32. A. Read, M. Mathioudakis, J. G. Doyle, et al., "Magnetic flux cancellation in Ellerman bombs," Astrophys. J. **823**, 110 (2016).
33. R. J. Rutten, L. H. M. Rouppe van der Voort and G. J. M. Vissers, "Ellerman bombs at high resolution. IV. Visibility in Na I and Mg I," Astrophys. J. **808**, 133 (2015).
34. R. J. Rutten, "Hα features with hot onsets I. Ellerman bombs," Astron. Astrophys. **590**, A124 (2016).
35. H. Socas-Navarro, V. Martinez Pillet, D. Elmore, et al., "Spectro-polarimetric observations and non-LTE modeling of Ellerman bombs," Sol. Phys. **235**, 75–86 (2006).
36. H. Socas-Navarro and H. Uitenbroek, "On the diagnostic potential of Hα for chromospheric magnetism," Astrophys. J. Lett. **603**, L129–L132 (2004).
37. G. Valori, L. M. Green, P. Demouli, et al., "Nonlinear force-free extrapolation of emerging flux with a global twist and serpentine fine structures," Sol. Phys. **278**, 73–97 (2012).
38. G. J. M. Vissers, L. H. M. Rouppe van der Voort and R. J. Rutten, "Ellerman bombs at high resolution. II. Triggering, visibility, and effect on upper atmosphere," Astrophys. J. **774**, 32 (2013).
39. H. Watanabe, R. Kitai, K. Okamoto, et al., "Spectropolarimetric observation of an emerging flux region: triggering mechanisms of Ellerman bombs," Astrophys. J. **684**, 736–746 (2008).
40. H. Watanabe, G. Vissers, R. Kitai, et al., "Ellerman bombs at high resolution: 1. Morphological evidence for photospheric reconnection," Astrophys. J. **736**, 71 (2011).
41. Th. G. Zachariadis, C. E. Alissandrakis and G. Banos, "Observations of Ellerman bombs in Hα," Sol. Phys. **108**, 227–236 (1987).

Translated by D. Safin